Ocean Engineering 243 (2022) 110189

Contents lists available at ScienceDirect

Ocean Engineering

journal homepage: www.elsevier.com/locate/oceaneng

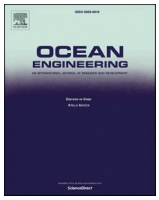

Wave loads on high-rise pile cap structures and mitigation approach

Ling Chen [a,b], Jifu Zhou [a,b,*], Jinlong Duan [a,**], Xu Wang [a], Yiqin Xie [a,b]

[a] Key Laboratory for Mechanics in Fluid Solid Coupling Systems, Institute of Mechanics, Chinese Academy of Sciences, Beijing, 100190, China
[b] School of Engineering Sciences, University of Chinese Academy of Sciences, Beijing, 100049, China

ARTICLE INFO

Keywords:
High-rise pile cap foundation
Wave impact loads
Cap bottom elevation
Structural improvement

ABSTRACT

A novel type of foundation, a high-rise pile cap structure, was proposed to support offshore wind turbines in China. It is unique because the upper cap is now and then partially submerged or totally exposed in the air. The wave force of this unique structure is not well understood yet. In this paper, a fully nonlinear numerical wave tank is established to deal with this problem based on Navier-Stokes equations and volume of fluid technique. The wave impact loads on the structure and their mechanism are revealed. Modifications of the cap bottom elevation are considered to explore its influence on direct and indirect wave impact loads on the lower piles. The wave impact load on the most dangerous pile is detected high if the cap bottom is at the still water level or close to the wave crest level, and small impact load is found while the cap bottom is at the height of half wave crest. Attempts of structural improvement are considered to reduce the wave impact loads on the piles. The wave impact load can be notably reduced by opening air vents in the cap together with lifting the bottom of the inner part of the cap.

1. Introduction

The Donghai Bridge Wind Farm was built by China as the first large-scale offshore wind farm in Asia a decade ago. A high-rise pile cap structure is utilized for the foundation of wind turbines in this wind farm, which is totally distinct from the monopile foundations widely used in the North Sea. A circular platform of 14 m diameter and eight supporting piles of 1.7 m diameter are included in this type of foundation. Meanwhile, the platform is also equipped with a high vertical tower with a 3.4 MW wind turbine fixed at its top. This new concept of wind turbine foundation is generally proposed according to the environmental and business factors in the East China Sea, such as the hydrogeological and weather conditions. As is reconnoitered, the seabed in the East China Sea is covered with multi-layer soft clay, the thickness of which can be up to more than 25 m. If a large diameter monopile or tripod foundation is installed on such seabed, a wide range of surface hardening is required to protect the seabed near the foundations for large installation capacity so that the safety and stability of offshore wind turbine structures on this soft clay could be guaranteed. However, this could result in an adverse impact on marine ecology and be against the environmental protection requirements (Chen et al., 2016). Another factor is due to the severe weather condition such as typhoon, more stringent criteria for the structure's strength and stability are required there. Furthermore, there is a necessity to prevent the foundation from ship collisions because of the busy fairway across the wind farm. Based on the aforesaid factors, the new foundation is concepted and designed for the engineering application.

No doubt that there exist many advantages for the new foundation over other traditional supporting systems, such as high stiffness, manageable risk, economical cost, anti-collision, environmental hospitality, etc. (Chen et al., 2016). Therefore, such a novel foundation provides a solid support to the offshore wind turbines (Lin, 2007) and has been proved a great success in China. However, some examinations for the foundation are still necessary in order to promote its robustness, especially under the circumstance of extreme conditions. The extreme wave loads on the foundation is worthy of further investigation. Since the foundation structures are very complex, the extreme waves could exert strongly nonlinear effect on these structures. In addition, unlike the foundation totally or partly submerged in the water, the cap is located near the still water level for the sake of anti-collision. This particular requirement makes the cap bottom periodically expose in the air when wave trough passes and submerge in water when wave crest

* Corresponding author. Key Laboratory for Mechanics in Fluid Solid Coupling Systems, Institute of Mechanics, Chinese Academy of Sciences, Beijing, 100190, China.
** Corresponding author.
E-mail addresses: zhoujf@imech.ac.cn (J. Zhou), duanjl@imech.ac.cn (J. Duan).

https://doi.org/10.1016/j.oceaneng.2021.110189
Received 20 July 2020; Received in revised form 9 November 2021; Accepted 10 November 2021
Available online 26 November 2021

passes. Consequently, the wave load exerting on such a novel type of foundation is more complicated. And the wave load could not be accurately estimated by the traditional methods, i.e. the Morison equation and the diffraction theory.

As a matter of fact, the wave loads exerting on the high-rise pile cap foundation consists of both the ordinary wave force and the unusual load resulted from surface wave impacting the bottom of the cap. And the latter one could make a large contribution to the total wave loads. There have been some related researches which were carried out on wave-in-deck loads. Bredmose and Jacobsen (2011) performed a numerical simulation to study the wave impacts on a monopile and found that the wave has a subsequent vertical effect on the inspection platform. Schellin et al. (2011) developed a modern CFD technique to predict the loads on a typical jack-up platform, considering the wave-in-deck load acting on the hull suffering freak waves particularly. Besides, Seiffert et al. (2014) conducted a variety of laboratory experiments and calculations using the InterFoam solver in OpenFOAM, focusing on the horizontal and vertical forces acting on a two-dimensional horizontal plate due to solitary waves.

It should be noted that the wave-in-deck load is not same as that exerting on the high-rise pile cap foundation. The wave-in-deck load is generally referred to as the force caused by direct impacting of a wave on a structure. Yet the wave loads on the high-rise pile cap foundation consist of two components. One is the wave-in-deck load acting on the upper cap. The other is the load exerting on the lower piles, which is significantly influenced by the high speed jet-like flow under the near bottom of the cap and the unusual pressure field resulted from wave impacting on the cap bottom. That is why the wave loads on the lower piles cannot be accurately calculated by using mature theories or traditional formulas as found in Offshore Standards. Fortunately, the latest CFD techniques are effective and robust enough in modeling wave-structure interactions. Once the pressure field is accurately obtained with CFD approach, the wave loads acting on the piles can be directly and effectively calculated by integrating the pressure over the wet surface of the piles.

Recently, scholars have dedicated themselves to the numerical simulation of nonlinear waves or extreme waves and their interaction with structures by using CFD. In these works, the wave generation and absorption are extensively studied based on CFD (Morgan et al., 2010; Jacobsen et al., 2012; Higuera et al., 2013; Altomare et al., 2017). Then the wave-structure interaction between a variety of structures and waves has also been paid much attention, such as the vertical cylinders (Paulsen et al., 2014a; Chen et al., 2014; Hu et al., 2016; Lin et al., 2017; Zheng et al., 2018) and the surface-piercing bodies (offshore floating bodies, coastal bridge decks) (Stansberg et al., 2005; Li and Lin, 2012; Higuera et al., 2014; Seiffert et al., 2015; Cannata et al., 2019). In particular, Chen et al. (2018) carried out numerical simulations of the interaction between the high-rise pile cap structure and an extreme wave, figuring out direct and indirect consequences of wave impacting on the cap bottom which was overlooked in the design of the structure. They revealed the difference of the wave loads on the lower plies whether wave impacting on the cap bottom occurs. The magnitude of wave impact loads under certain wave climate mainly depends on the geometry and height of the structures. Therefore, the wave height, wave length, cap dimension and submerged depth have significant influences on wave loads (Kleefsman et al., 2005; Iwanowski et al., 2009; Hayatdavoodi et al., 2014; Deng et al., 2019). Cuomo et al. (2009) and Seiffert et al. (2015) found that the wave impact loads can be effectively reduced by appropriate structural optimization during engineering design.

The present work aims to investigate the variation of the wave loads on the high-rise pile cap foundation with the elevation of the cap bottom based on our previous work as reported in Chen et al. (2018) and explore possible measures in structure design to mitigate the wave loads due to the wave impacting effect. The next Section briefly summarizes the numerical model and its validation as was published in Chen et al. (2018). Section 3 covers two parts. The first part examines the wave loads on the foundation with different cap bottom elevations. The second part discusses the mitigation measurements and the mechanisms of wave loads on the lower piles by considering opening air vents in the cap and lifting the bottom of the inner part of the cap. Finally, some conclusions are drawn in Section 4.

2. Numerical approach

The incompressible Navier-Stokes solver named interFoam is adopted to simulate the fully nonlinear wave interaction with the high-rise pile cap structure. This solver is available in the OpenFOAM Toolbox and is designed for simulating the evolution of the interface between two phases at constant temperature. For fully nonlinear wave conditions and complex interaction, the Navier-Stokes equations can be an appropriate choice to describe large deformations of the free surface and even wave breaking especially near the structures.

2.1. Governing equations

The Navier-Stokes equations can be written as:

$$\nabla \cdot \boldsymbol{U} = 0 \tag{1}$$

$$\frac{\partial \rho \boldsymbol{U}}{\partial t} + \nabla \cdot (\rho \boldsymbol{U})\boldsymbol{U} - \nabla \cdot \left(\mu_{eff} \nabla \boldsymbol{U}\right) - \nabla \boldsymbol{U} \cdot \nabla \mu_{eff} = -\nabla p^{*} - (\boldsymbol{g} \cdot \boldsymbol{x}) \nabla \rho \tag{2}$$

where ρ and μ_{eff} are the fluid density and the dynamic viscosity respectively, $\boldsymbol{U}$ and $\boldsymbol{x}$ are the fluid velocity and position vectors respectively, $\boldsymbol{g}$ is the acceleration due to gravity pointing downwards, p^{*} is the modified pressure defined as

$$p^{*} = p - \rho \boldsymbol{g} \cdot \boldsymbol{x} \tag{3}$$

where p is the pressure. Using the modified pressure has advantages of specifying the pressure on the boundary and stabilizing numerical simulations (Rusche, 2002).

A combined PISO-SIMPLE (PIMPLE) algorithm proposed by Jasak (1996) is applied to solve the velocity-pressure coupling. In this scheme, the Semi-Implicit Method for Pressure-Linked Equations (SIMPLE) is adopted to calculate the pressure iteratively from velocity on local mesh based on the Navier-Stokes equations, and the Pressure Implicit Splitting Operator (PISO) is used to modify the pressure-velocity system.

The interface between the two fluids is captured through the VOF technique (Hirt and Nichols, 1981) by using the volume fraction to define the volume portion of each phase occupying in the cell. In this method, a unified equation is applied to integrate the air and water phase calculations by the volume fraction α, which can be written as

$$\frac{\partial \alpha}{\partial t} + \alpha \nabla \cdot \boldsymbol{U} + \alpha(1-\alpha) \nabla \cdot \boldsymbol{U}_r = 0 \tag{4}$$

where $\boldsymbol{U}_r$ is a relative compression velocity, which is only used in the free surface in order to remove the unphysical values. This is a modified approach with an advanced model proposed by Berberović et al. (2009). In this model, an additional convective term, which originates from modeling the velocity in terms of a weighted average of the corresponding liquid and gas velocities, is applied to deal with the free surface. And the numerical diffusion of the interface is artificially prevented by adopting the relative compression velocity, which has been described in detail by Weller et al. (1998) and Berberović et al. (2009).

The motions of air and water are calculated at the same time as a mixed flow, and the local density and dynamic viscosity can be determined as

$$\rho = \alpha \rho_w + (1-\alpha)\rho_a \tag{5}$$

$$\mu = \alpha \mu_w + (1-\alpha)\mu_a \tag{6}$$

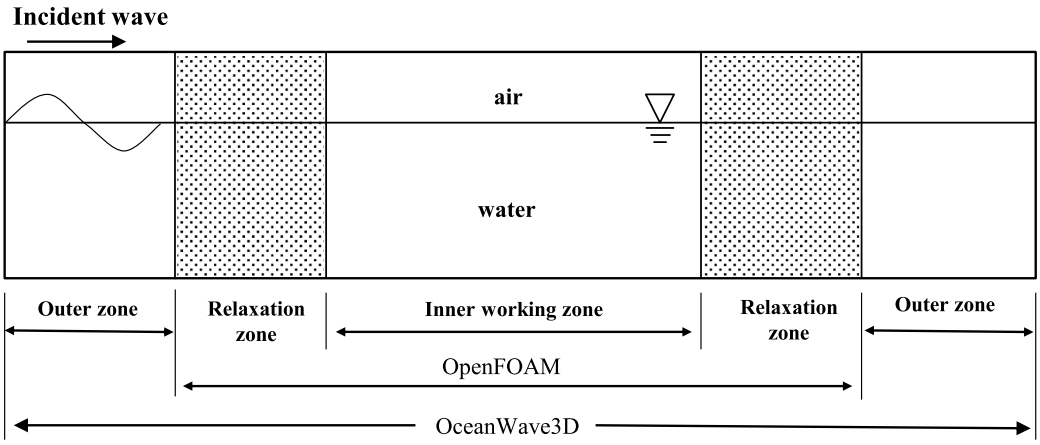

Fig. 1. The sketch of coupled numerical wave tank model.

where subscripts w and a refer to water and air respectively.

The SST $k-\omega$ turbulence model (Menter, 1994) is employed to simulate the boundary layer flow near the cylinder. By doing this, the effect of water viscosity on the wave loads on the cylinder is taken into account during the simulation.

2.2. Numerical wave tank

A three-dimensional numerical wave tank is established here. The symmetry boundary conditions are applied for the side walls while the no-slip and no fluid penetration boundary conditions are used for the bottom wall of the tank. And the atmosphere pressure is adopted as the pressure on the top boundary. The inlet boundary conditions should be paid special attention. The target wave theory and the expected wave parameters are utilized to specify water particle velocities and surface elevation. No-slip and no fluid penetration boundary is also applied on the outlet boundary. As for the cylinder surface, no-slip boundary conditions are specified.

During the simulation, the target wave theory and the expected wave parameters should be utilized to specify the values of water particle velocities and surface elevation. Thus, wave generation and absorption are achieved by using a relaxation technique (Paulsen et al., 2014a), which is coupling fully nonlinear potential wave solver OceanWave3D (Engsig-Karup et al., 2009) and fully nonlinear wave generation and absorption program waves2Foam (Jacobsen et al., 2012). Based on the aforesaid method, the target wave can be easily simulated in a relatively small computational domain with no worry about wave reflections. Since specific wave conditions can be coupled by this means, this numerical wave tank technique is chosen here.

The reflected or internally generated waves are commonly removed by the relaxation technique. As illustrated in Fig. 1, In the inlet and outlet zones, the relaxation zones are utilized. Within the relaxation zone, the water particle velocity $\boldsymbol{U}$ and surface elevation η are relaxed in each time step by the following function,

$$\Phi(x,t) = \xi(\sigma)\Phi(x,t)_{target} + (1-\xi(\sigma))\Phi(x,t)_{computed} \tag{7}$$

where Φ represents either $\boldsymbol{U}$ or η. $\Phi(x,t)_{target}$ is the value given by target wave theory parameters. $\Phi(x,t)_{computed}$ is the value computed by Eqs. (1), (2) and (4). $\xi(\sigma)$ is the relaxation factor defined as

$$\xi(\sigma) = 1 - \frac{\exp(\sigma^{3.5}) - 1}{\exp(1) - 1}\ ,\ \sigma\varepsilon[0,1] \tag{8}$$

where σ is the normalized horizontal coordinate along the relaxation zone. The value of σ is zero at the position close to the outer zone and unity close to the inner working zone. In general, the relaxation zones should be long enough so that no wave re-reflection can be guaranteed. And the length of the relaxation zones should exceed the reflecting wave length.

2.3. Validation

Before simulation, validation work is required in order to ensure the accuracy of the numerical wave tank. Although the relaxation technique for wave generation and absorption have been validated by Jacobsen et al. (2012) and Paulsen et al. (2014b), further validations of wave elevation and wave forces have been carried out by Chen et al. (2018). The detailed results of all these validations can be referred to Chen et al. (2018) and will not be elaborated here, but are summarized as follows.

The validation of wave elevation was made by comparing the numerical free surface elevation of a nonlinear wave with the theoretical predictions of stream function theory, exhibiting extremely good agreement. As for wave force validation, it is necessary in the present work to consider two kinds of wave force, the conventional wave force and the wave impact force. The conventional wave force was validated by investigating the force on a cylinder by a nonlinear wave. And the simulated conventional wave force agrees well with that calculated by Morison equation. The wave impact force was validated by investigating the impact load on a 3D box by a 3D dambreak wave. The mechanism of wave impacting the cap in the present paper is highly similar to the dambreak wave impacting a box because both are free surface impinging a structure forming impact load. Good agreement was obtained between the simulated time series of pressure and the laboratory results of Kleefsman et al. (2005). In particular, the impact pressure peaks were accurately captured. In addition, with the high-rise pile cap structure considered, the mesh configurations for grid convergence were also studied.

3. Results and discussion

The present research is a continuation of our previous one by Chen et al. (2018), in which we found that the wave load on piles are quite different whether the cap is included. During the previous research, the maximum horizontal wave load on all the piles with the cap was found increased by 30% compared with those without the cap. The conventional Morison formula and diffraction theory generally underestimate the wave loads on the piles and the cap. In this paper, the wave parameters and structure setting studied are exactly similar to those in Chen et al. (2018). Some important parameters are briefly introduced again for easy understanding. The Donghai Bridge Wind Farm, East China Sea, is located in the shallow water area with a depth of 11 m. In

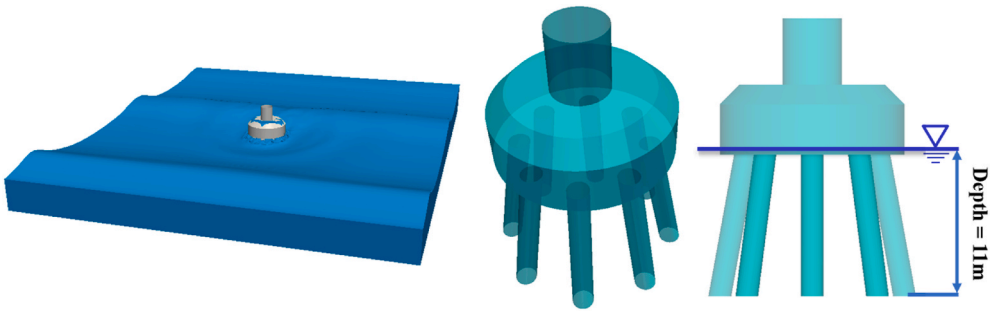

Fig. 2. The simplified physical domain with a high-rise pile cap structure in it.

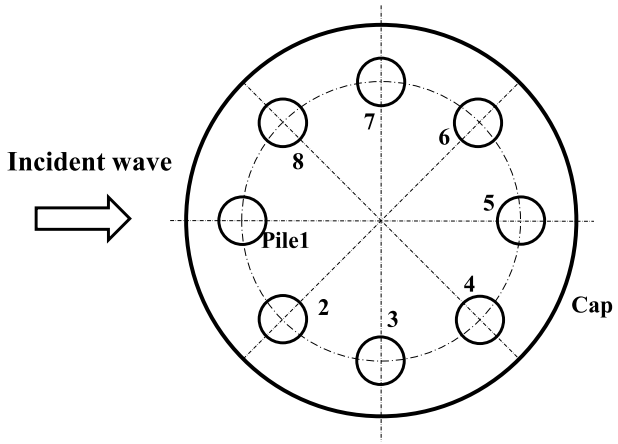

Fig. 3. The locations relative to the incident wave of the piles on which the numerical pressure is measured.

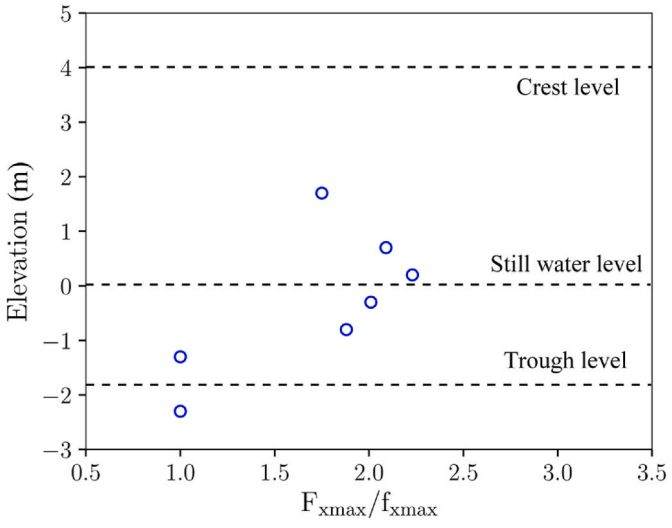

Fig. 4. The ratio $F_{x\,max}/f_{x\,max}$ on Pile 5 versus cap bottom elevation (H = 5.8 m).

the present study, the designed wave height, $H_{1\%}$ (only 1% wave heights in a group of measured wave heights are higher than $H_{1\%}$), with 50-year return period is chosen here. The wave parameter is set to close to the limit of wave breaking, with the wave length 75 m, the wave height 5.8 m and the period 7.8 s. This nonlinear wave is achieved by stream function theory with twenty-order truncation (Fenton, 1988). These are exactly the in-situ hydrodynamic environments for the wind farm.

As sketched in Fig. 2, the simplified physical domain and the

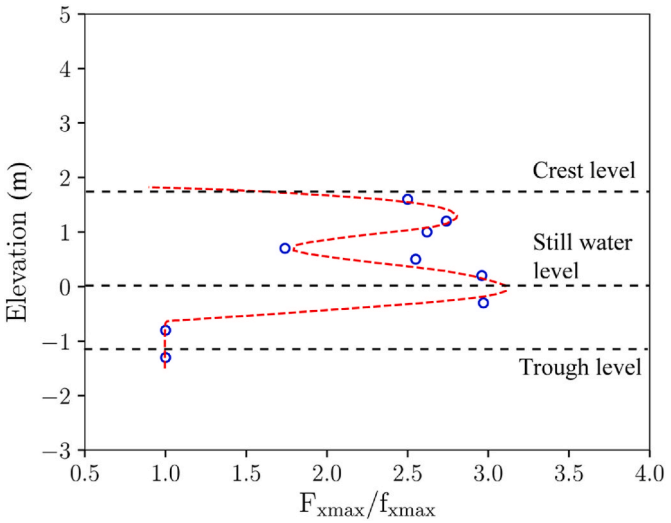

Fig. 5. The ratio $F_{x\,max}/f_{x\,max}$ on Pile 5 versus cap bottom elevation (H = 2.83 m).

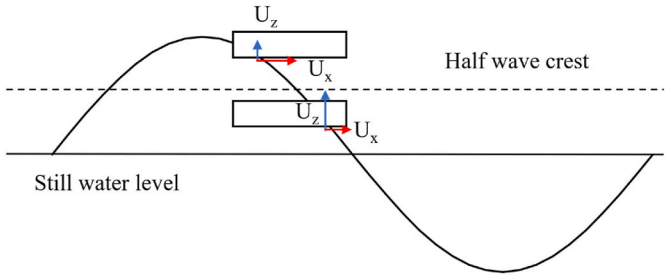

Fig. 6. Sketch of horizontal and vertical wave velocities with different cap bottom elevations when wave impacts cap bottom (higher and lower than the elevation of half wave crest).

structure supporting offshore wind turbines are displayed. The structure consists of a circular platform, a tower and eight inclined supporting piles with diameters of 14 m, 4.5 m and 1.7 m respectively. Besides, the eight inclined supporting piles are with a slope ratio of 5.5 to 1. The surface piercing cap, with the bottom elevation of −0.3 m to the still water level, is comprised of two parts (Fig. 2). The lower part is a cylinder with height of 3 m, and the upper one is a frustum of a cone with 1.5 m height. Eight inclined piles are evenly mounted along a circular of 5 m radius on the bottom of the cap. The pile configuration is set as shown in Fig. 3.

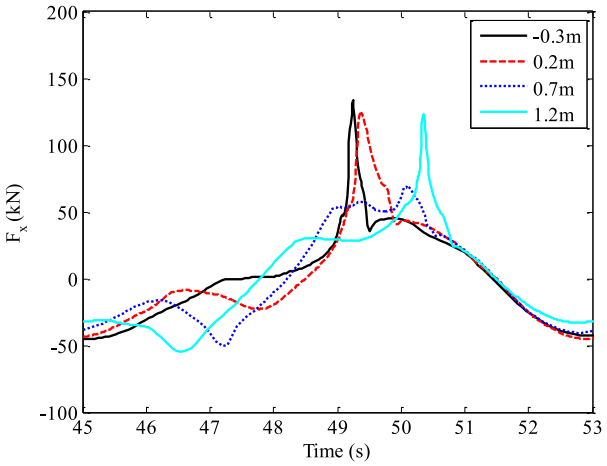

Fig. 7. Horizontal force on Pile 5 for $H = 2.83$ m with different cap bottom elevations.

3.1. Wave impact loads on the piles with various cap bottom elevations

While a wave impacts the high-rise pile cap foundation, complicated wave forces can be generated and act on the structure. These wave forces could have a great effect on the stability of the structure. It is thus of great significance to investigate the method of reducing the impact load. The air gap between the cap bottom and the still water level have been proved to have a notable influence on the wave impact load on the piles when the wave parameters are specified (Deng et al., 2019). Therefore, the cap bottom elevation is regarded as an important parameter in structure design. Let us keep all the previous computational configurations unchanged except for the elevation of the cap bottom. The wave loads on piles in seven cases with different cap bottom elevations are investigated: −2.3 m, −1.3 m, −0.8 m, −0.3 m, 0.2 m, 0.7 m, 1.7 m. As the wave force on Pile 5 is found largest among all the piles, Pile 5 is regarded as the most dangerous pile in the whole structure (Chen et al.,

Table 1
Configurations for various structural optimization.

	Vent type	Vent size	Percent opening χ	Z_{cb}
Test 1	Circular holes	(D = 1 m) × 8 $R_{location}$ = 3.25 m	4.63%	−0.3 m
Test 2	Circular groove	R_{inner} = 3.475 m R_{outer} = 3.75 m	4.63%	−0.3 m
Test 3	Circular groove	R_{inner} = 2.75 m R_{outer} = 3.75 m	15.04%	−0.3 m
Test 4	Circular groove	R_{inner} = 3.475 m R_{outer} = 3.75 m	4.63%	2 m
Test 5	Circular groove	R_{inner} = 2.75 m R_{outer} = 3.75 m	15.04%	2 m

D is the diameter of the circular holes.
$R_{location}$ is the radius of the circle formed by the centers of the eight holes.
R_{inner} and R_{outer} are the inner and outer radius of the circular groove, respectively.
Z_{cb} is the height of the cap bottom surrounded by the holes or grooves to the still water level.

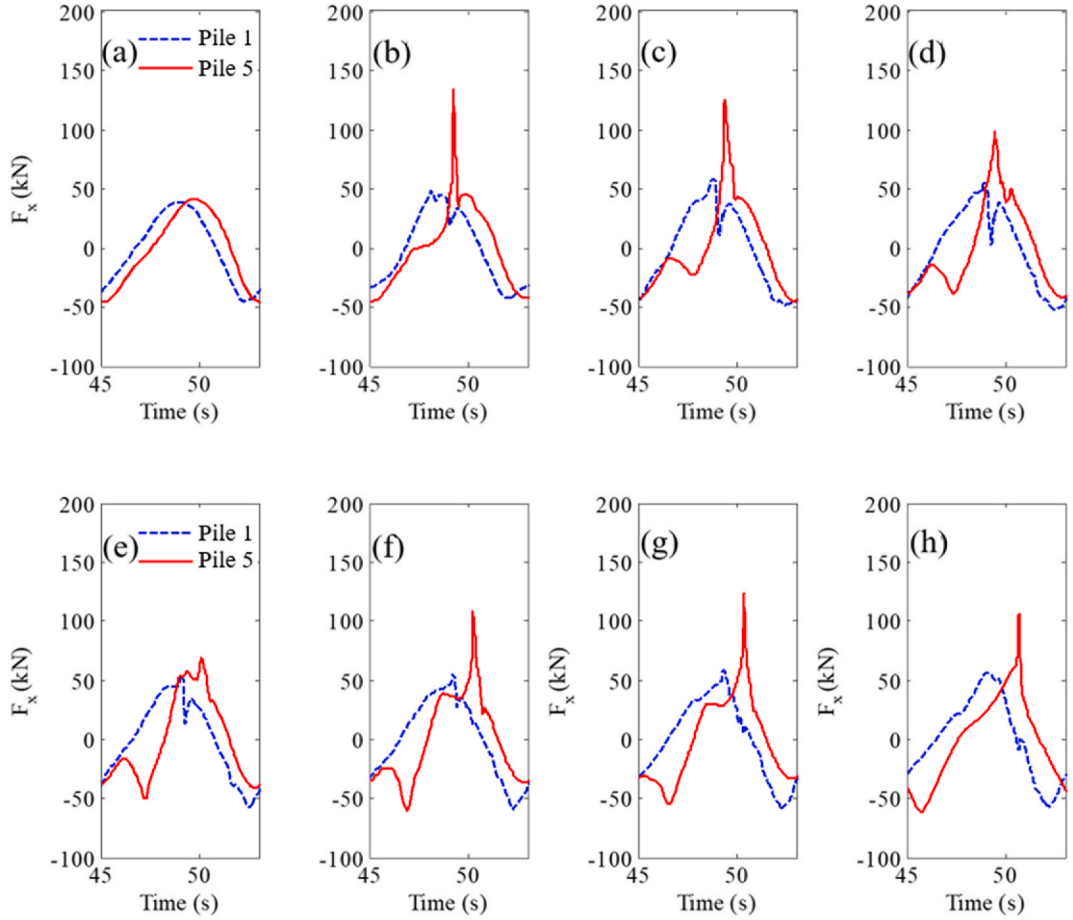

Fig. 8. Horizontal force on Pile 1 and Pile 5 for $H = 2.83$ m with different cap bottom elevations: (a) −0.8 m; (b) −0.3 m; (c) 0.2 m; (d) 0.5 m; (e) 0.7 m; (f) 1.0 m; (g) 1.2 m; (h) 1.6 m.

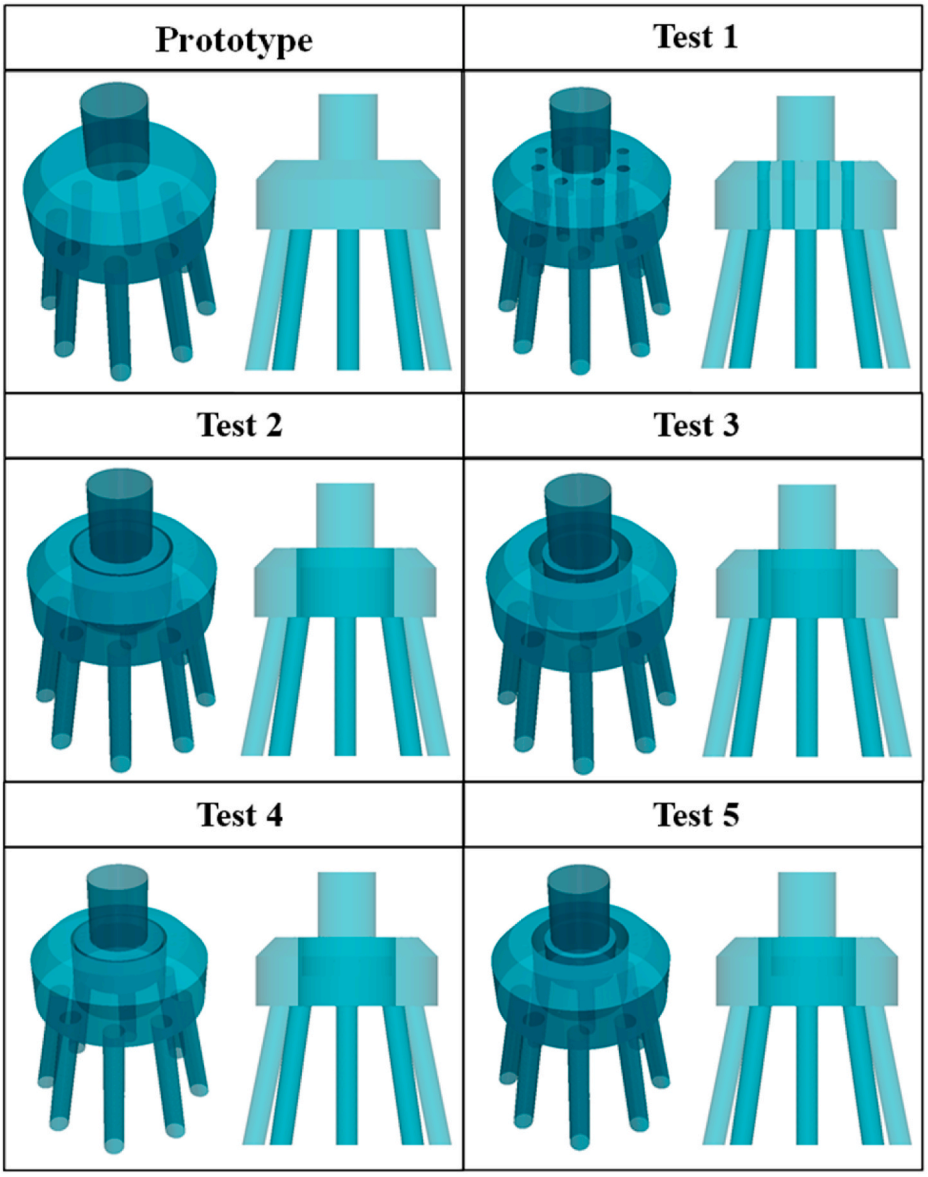

Fig. 9. Sketches of various structural improvements.

2018). Therefore, the wave force on Pile 5 is mainly focused and discussed here. Then the maximum horizontal force on Pile 5 is analyzed and Fig. 4 shows the ratio $F_{x\,max}/f_{x\,max}$ versus the cap bottom elevation with wave height $H = 5.8$ m, where $F_{x\,max}$ and $f_{x\,max}$ represent the maximum horizontal forces with and without the cap, respectively. Note that the wave impact load is included in $F_{x\,max}$.

As indicated in Fig. 4, this ratio value $F_{x\,max}/f_{x\,max}$ with most of the cap bottom elevation apparently exceeds 1.0 when the cap bottom is impacted by the wave. When the elevation of the cap bottom is located at the height of −2.3 m or −1.3 m, there is no obvious increase for the wave impact loads. This can be explained by that the wave impact has little effect on the horizontal wave force as the cap bottom is almost submerged into the water with the cap bottom elevation at the height of −2.3 m or −1.3 m. However, the wave impact loads on Pile 5 increase notably when the cap bottom elevation is increased up to around the still water level, ranging from −0.8 m to 0.7 m. When the cap bottom elevation approaches to the still water level, the value of $F_{x\,max}/f_{x\,max}$ is higher than 2.0. With the increase of the cap bottom elevation around the still water level, the value of $F_{x\,max}/f_{x\,max}$ firstly increases and then decreases. And its maximum value of 2.25 is observed when the cap bottom elevation is at the height of 0.2 m. The evident increase of $F_{x\,max}/f_{x\,max}$ here can be attributed to the high speed jet-like flow under the near bottom of the cap and high pressure field generated by wave impact. As the wave free surface impacts the cap bottom vertically, the water particle velocity direction is changed due to the impact, generating a horizontal high speed water jet under the bottom of the cap. Then the high speed jet-like flow impacts Pile 5, magnifying the wave force on Pile 5. When the cap bottom elevation is increased up to higher than 1.7 m, the wave free surface impacts the cap bottom with small vertical velocity. Consequently, the jet-like flow under the bottom of the cap is generated with smaller speed under this circumstance. Besides, there is nearly no high-pressure zone occurring. Hence, relatively small horizontal forces are detected on Pile 5 with such cap bottom elevation. It should be noted that the extreme ratio of $F_{x\,max}/f_{x\,max}$ might occur at slightly different values of the cap bottom elevation because the cases of different cap bottom elevations are limited here.

Apart from the effect of the cap bottom elevation, $F_{x\,max}/f_{x\,max}$ also depends on the wave height. Based on the measured wave height in the Donghai Bridge Wind Farm, the average wave height of 2.83 m is taken into account. And the wave loads on Pile 5 are investigated in nine cases

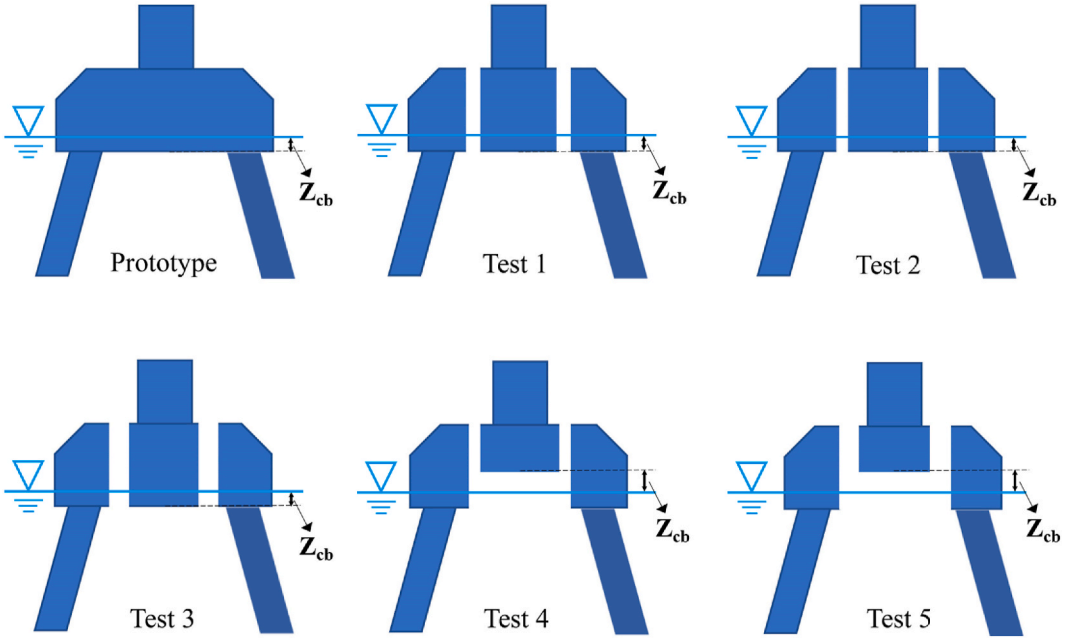

Fig. 10. Sketches of structural section in the vertical plane that cuts Pile 1 and Pile 5.

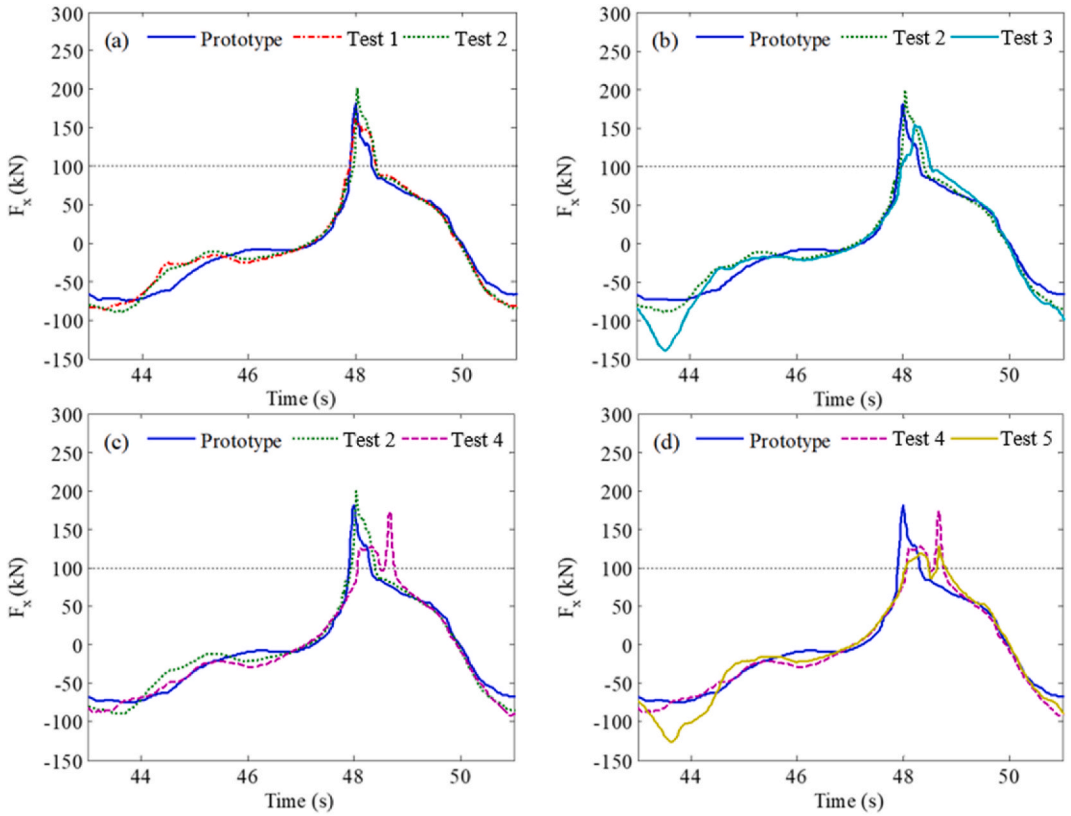

Fig. 11. Time histories in one wave period of the horizontal force on Pile 5. (a) Prototype, Tests 1 and 2; (b) Prototype, Tests 2 and 3; (c) Prototype, Tests 2 and 4; (d) Prototype, Tests 4 and 5.

with different cap bottom elevations: −1.3 m, −0.8 m, −0.3 m, 0.2 m, 0.5 m, 0.7 m, 1.0 m, 1.2 m, 1.6 m. The values of $F_{x\,max}/f_{x\,max}$ are presented in Fig. 5. It is also found that when the cap bottom elevation is near the trough level, the impact load on Pile 5 is not evident, leading to the value of $F_{x\,max}/f_{x\,max}$ equal to approximately 1.0. When the cap bottom elevation is located at around the still water level, Pile 5 undergoes serious impact loads. As a result, the value of $F_{x\,max}/f_{x\,max}$ in this case can be up to about 3.0, which is higher than that with 5.8 m wave height. The increase of $F_{x\,max}/f_{x\,max}$ is also caused by the high speed jet-like flow and high pressure field under the cap bottom. But it should be noted that the high pressure field plays a dominant role here.

When the cap bottom elevation continues to rise, the impact load on

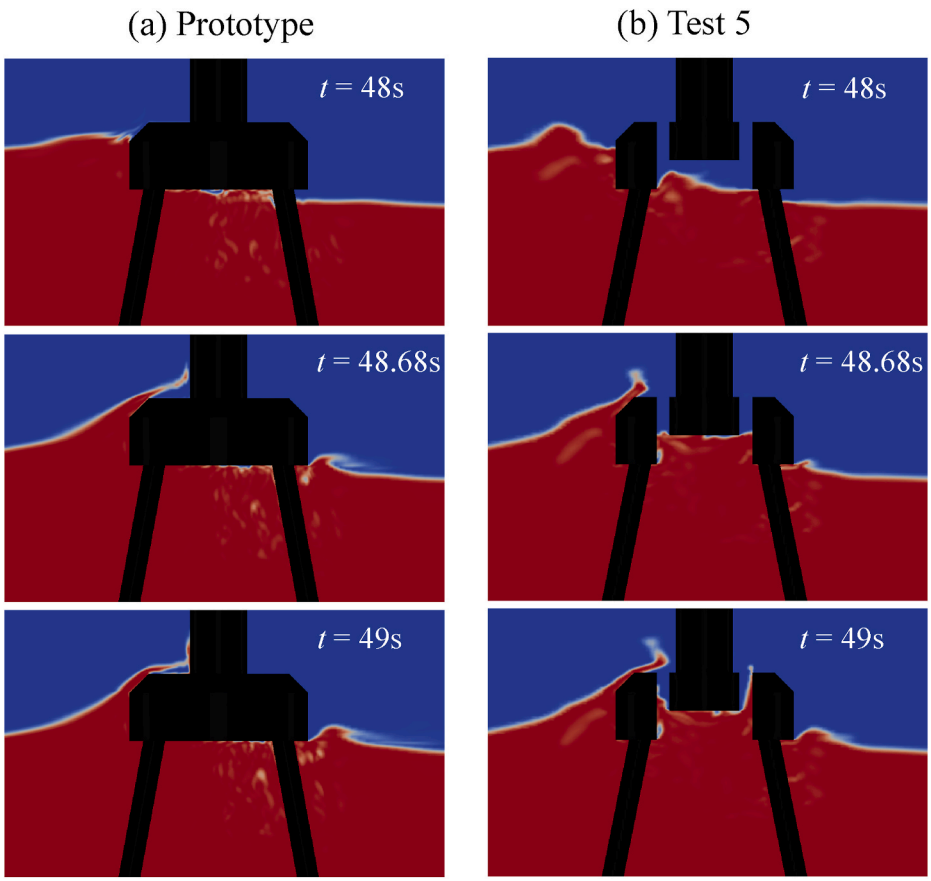

Fig. 12. Evolution of wave free surface in Prototype and Test 5.

Pile 5 is rapidly reduced, which proves that the effect of the high speed jet-like flow and high pressure field begin to diminish at certain cap bottom elevation. But what should be also paid attention is that when the cap bottom elevation approaches to the crest level, the impact load becomes significant again (Fig. 5). This is obviously not due to the high-pressure zone mentioned above. It can be explained by that when the air gap between the cap bottom and the still water level is larger than half wave crest, the wave impacts the cap bottom with smaller vertical velocity component and higher horizontal velocity component, as shown in Fig. 6. In addition, the impact enhances the horizontal velocity, forming a horizontal water jet with higher velocity near the cap bottom. As a result, the water jet impacts Pile 5 directly, generating an instantaneous impact load. When the cap bottom elevation is higher than the crest level, the value of $F_{x\,max}/f_{x\,max}$ is equal to 1.0 again because of no wave impact at all. Therefore, $F_{x\,max}/f_{x\,max}$ varies with the cap bottom elevation in a way like the dashed curve as shown in Fig. 5. And the results prove that the wave impact loads cannot be ignored for medium wave height conditions.

Figs. 7 and 8 show the time series of the horizontal force on Pile 1 and Pile 5, where two peaks of each curve can be found in most cases. The first peak represents the indirect impact load resulted from the additional pressure increment, while the second one represents the direct impact load due to the horizontal high speed water jet. As is observed in Fig. 7, there exist high indirect impact load and very small direct impact load for the cases with small air gap. In contrast, small indirect impact load and large direct impact load can be detected for the cases with large air gap. When the air gap approximately equals to half wave crest, both kinds of impact load are relatively small, as shown in Fig. 8 (e). In addition, it can be found that Pile 1 mainly suffers the indirect impact load due to the high-pressure zone while the direct impact has little influence on it. These characteristics can be used as a reference to distinguish these two kinds of impact load from each other. But it should be addressed that the air gap cannot be too large in order for the requirement of anti-collision. Therefore, the cap bottom elevation that is as high as half wave crest is recommended so that the impact forces on the piles are minimized.

3.2. *The structural improvement schemes for reducing wave load*

As the impact load can cause very large transient local stress of the piles, it is considered as a disadvantage of the safety control of the foundation structure. Therefore, in order to guarantee the safety of the whole foundation, improvement of structural configuration design is usually adopted to reduce the impact load. It has proved that design with air vents is an effective way to reduce the impact load on the bridge decks (Cuomo et al., 2009; Azadbakht and Yim, 2016). Although the cap bottom elevation has been proved to have an important effect on the impact load in section 3.1, it cannot be enlarged without consideration of anti-collision. Therefore, some improvement of structural configuration is proposed here while the combination of reducing the impact load and meeting the anti-collision requirement is taken into account.

Based on the considerations above, the impact loads with five different structural configurations are investigated. And the parameters of these five configurations are listed in Table 1. Accordingly, the models are sketched in Fig. 9 while the model section in the vertical plane that crosses Pile 1 and Pile 5 is illustrated in Fig. 10. For all tests, the opening percentage is defined as the ratio of the vent area to the total cap bottom area. Z_{cb} in Table 1 represents the height of the cap bottom surrounded by the holes or grooves relative to the still water level, as shown in Fig. 10. The detailed sizes of the holes and grooves in different tests are presented in Table 1. For Tests 1, 2 and 4, the opening percentage is 4.63% while it is set up to 15.04% in Tests 3 and 5. Besides, eight

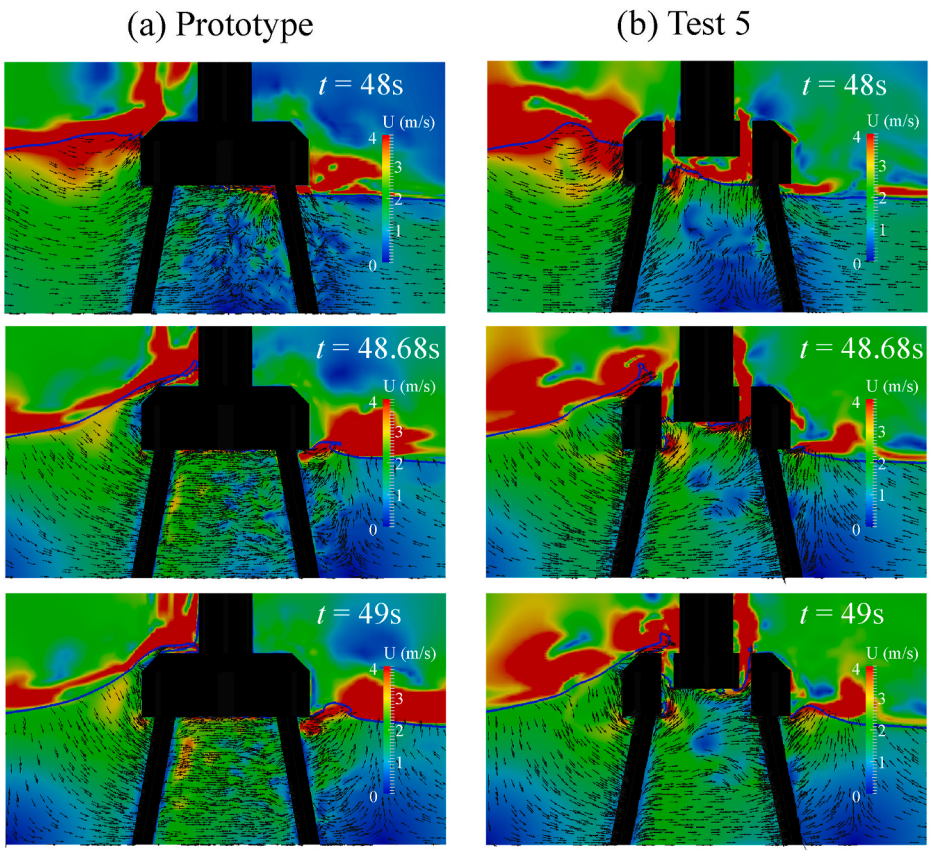

Fig. 13. Evolution of velocity filed in Prototype and Test 5.

Table 2
The reduction ratio of impact load on Pile 5 compared with the prototype foundation.

	Maximum horizontal impact force on Pile 5 (kN)	Reduction ratio
Prototype	101.3	0
Test 1	83.5	17.6%
Test 2	94.1	7.1%
Test 3	62.1	38.7%
Test 4	87.6	13.5%
Test 5	29.3	71.1%

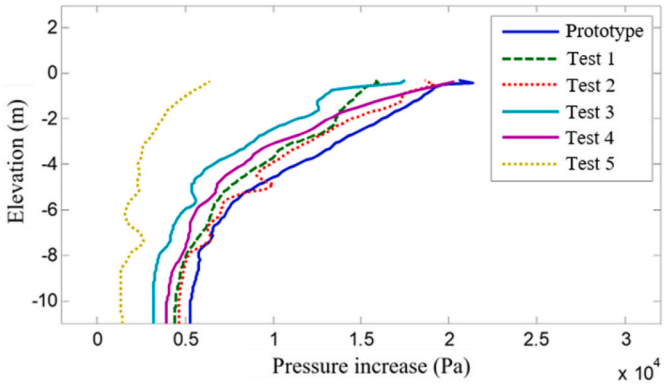

Fig. 14. Pressure increase along the central line of the foundation with different cap bottom elevations in each test.

circular holes penetrate vertically through the cap in Test 1. And a circular groove is considered for Tests 2, 3,4 and 5 (Fig. 9). Note that the inner cap bottom elevation surrounded by the circular groove in Tests 4 and 5 is elevated up to 2 m and those in other tests are maintained equal to −0.3 m, as shown in Fig. 10. It should be emphasized that the impact load with different structural configurations are mainly studied without consideration of connection or fixture between structural components here. Correspondingly, time histories of the horizontal forces on Pile 5 in these test cases, the most dangerous pile, are presented and compared in Fig. 11.

It can be seen from Fig. 11 (a) that the horizontal forces in Tests 1 and 2 are not evidently influenced compared with that on the prototype foundation, which indicates that the impact load is scarcely reduced when only the circular holes or groove with 4.63% opening percentage is considered. And the horizontal force in Test 3 is decreased compared to that for the prototype foundation and Test 2 (Fig. 11 (b)). The decrease manifests that with large opening percentage of 15.04%, the impact load on Pile 5 can be decreased by reducing the impact area. In other words, the horizontal force can be reduced by the decrease of the impact area on the cap bottom. In Fig. 11 (c) and (d), the effect of opening percentage together with lifting the inner cap bottom on the horizontal force is demonstrated. It can be seen from Fig. 11 (c) that there exist two peaks for the horizontal force in Test 4. The first peak appears nearly at the same time as the occurrence of that in prototype case and Test 2, but the value of the first peak is smaller compared with those in prototype case and Test 2. Then, the second peak emerges and reaches the maximum value of the horizontal force. This change can be attributed to the delayed impact caused by the elevation of the cap bottom surrounded by the groove. However, the horizontal force generated by the impact load in Test 4 is not as small as expected, which can be attributed to the high pressure field in water caused by the groove of small opening percentage. In this case, the air in the space between

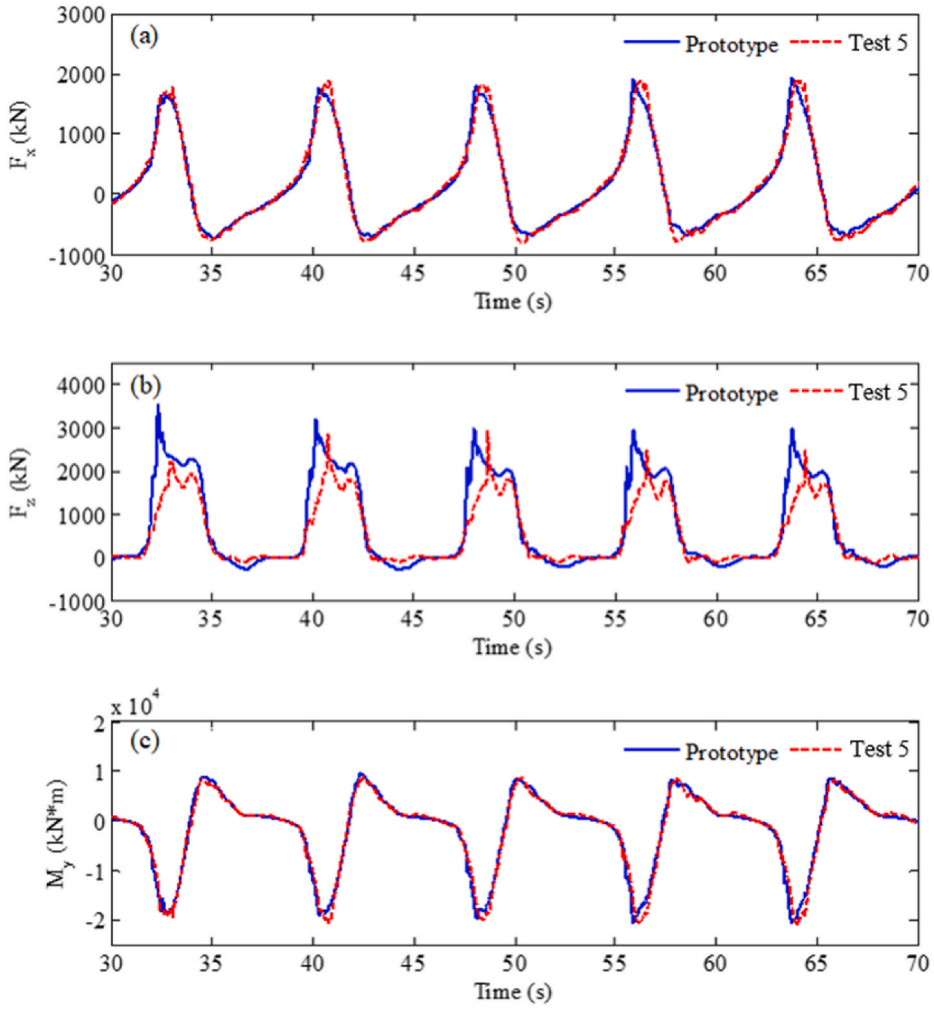

Fig. 15. Comparison of time histories of the total wave loads between Prototype and Test 5. (a) Horizontal wave force; (b) Vertical wave force; (c) Moment to the center at seabed.

the free surface and the surrounded cap bottom cannot be released in time, leading to high pressure in water in this area. It should be noted that as the velocity of air flow is not very high and there is no closed space trapping air in our simulation, compressibility of air has very little effect on the wave forces, as was pointed out by Seiffert et al. (2015) who compared the vertical and horizontal forces on a bridge deck calculated using compressible and incompressible Euler's equations. Therefore, air trapping effect is not considered during the present investigation. With the opening percentage enlarged, the air can be vented instantaneously, ensuring low pressure of water in the space between the free surface and the surrounded cap bottom. As a result, small horizontal force generated by the impact load can be detected on Pile 5. However, the horizontal force is observed notably reduced when there exists large circular groove and inner cap bottom elevation in Test 5, as shown in Fig. 11 (d), which implies that the impact load is evidently decreased with large opening vents and high elevation of the surrounded cap bottom.

In addition, the values of the negative horizontal forces in Tests 3 and 5 are higher than those in other cases, as shown in Fig. 11 (b) and (d). However, the absolute value of the negative horizontal force in either Test 3 or Test 5 is still smaller than the positive one.

From Fig. 11 (d), it can be seen that the peak of the horizontal force on Pile 5 of prototype foundation appears at $t = 48$s, without a second peak ensuing. However, in Test 5, the second peak emerges at $t = 48.68$s in company with the first one at $t = 48$s. Besides, the occurrence of the horizontal force peaks almost appears at the same moment in each test. This phenomenon can be explained by the evolution of wave-structure interaction displayed in Fig. 12, where the evolution of the wave-structure interaction for prototype foundation and Test 5 is illustrated. As seen in Fig. 12 (a), when the wave is approaching to the prototype structure, the wave free surface firstly elevates and then begins to touch the cap bottom of the prototype foundation at $t = 48$s. With the propagation of the wave, the cap bottom is impacted by the wave at $t = 48.68$s and the effect of impact continues at $t = 49$s. As a result, the horizontal wave velocity and the pressure under the cap bottom are increased, leading to high horizontal force exerting on Pile 5. However, the evolution of wave-structure interaction for the improved structure in Test 5 is quite distinct, as shown in Fig. 12 (b). At $t = 48$s, the wave surface elevates in the space surrounded by the circular groove without touching the surrounded cap bottom. Meanwhile, the air in the surrounded space is vented through the circular groove due to the elevation of the surface. As the wave propagates, the surrounded cap bottom is impacted by the wave at $t = 48.68$s, but still with a wave elevation in the circular groove. The late impact can account for the occurrence of the second peak for the horizontal wave force in Test 5. Additionally, the air in the surrounded space continues to flow out through the groove.

Correspondingly, the evolutions of velocity fields for prototype structure and Test 5 are demonstrated in Fig. 13. It has been proved for prototype structure that the water pressure under the cap bottom is increased as the rising wave is blocked by the cap bottom (Chen et al., 2018). As stated above, the vertical velocity of the flow is changed due to the blockage (Fig. 13), thereby causing that Pile 5 undergoes high horizontal force induced by both high speed jet-like flow and high pressure

field. As for Test 5, since there exists a space surrounded by the circular groove, no blockage in the inner area occurs for the rising wave at $t =$ 48s. Therefore, the wave velocity and pressure are scarcely changed and the wave surface keeps ascending with the wave propagation at this moment. As a consequence, the first peak of the horizontal force on Pile 5 in Test 5 is relatively smaller compared with that for prototype structure (Fig. 11). When the wave surface touches the surrounded cap bottom, wave impact occurs, during which high speed horizontal water jet appears due to the change of the wave vertical velocity. Correspondingly, the second peak of horizontal force emerges because of the impact load caused by the high speed jet-like flow (Fig. 11).

The reduction ratios of the impact load on Pile 5 in each test are shown in Table 2 by comparing with the prototype foundation. And the additional pressure increase detected along the central line of the foundation in different tests is plotted in Fig. 14. It can be found that pressure increase due to the wave impact in Test 5 is observed smallest among all cases. And the reduction ratio can be up to 71.1% in Test 5, as listed in Table 2. In addition, the time histories of total loads on the whole high-rise cap foundation of Prototype and Test 5 are shown in Fig. 15. As is demonstrated, the total horizontal wave force and moment in Test 5 are scarcely changed compared with the prototype. But the vertical wave force in Test 5 is detected reduced, which is favorable in practice. Therefore, it can be concluded that the impact load on Pile 5 can be notably reduced by structural improvement considering both large vent opening percentage and the elevation of the cap bottom surrounded by the vents.

4. Summary

Numerical calculations are performed to simulate the wave-structure interaction by using the fully nonlinear numerical wave tank technology. During the simulations, the wave loads on the high-rise pile cap foundation of offshore wind turbine used in the Donghai Bridge Wind Farm are mainly focused and studied. Compared to the conventional ones, the novelty of the investigated foundation lies in that the cap exposure in the air and partial submersion in the water occurs alternatively with the wave propagation. Correspondingly, modifications of cap bottom elevation are tested to explore the direct and indirect wave impact loads on the piles. And the wave load on the most dangerous pile is mainly analyzed and discussed. Meanwhile, some attempts of structural improvement are also carried out to reduce the wave impact load.

The cap bottom elevation has an unignorable effect on wave impact loads exerting on piles regardless of wave height. It is found that high impact load is detected on Pile 5 when the cap bottom elevation is located close to the still water level or approaching the crest level. The impact load exerting on Pile 5 is detected small when the cap bottom elevation is designed to locate at a height approximately equal to half wave crest. Therefore, a cap bottom that is positioned as high as half wave crest for design is recommended while the impact force on piles is taken into account.

In addition, structural improvement with air vents or elevation of the cap bottom surrounded by these vents is proved an effective method of reducing wave impact load on piles under the cap. And by opening air vents in the cap together with lifting the bottom of the inner part of the cap, the wave impact load on Pile 5 can be significantly reduced with a decrease up to about 71.1% here. Meanwhile, the total vertical wave force on the whole foundation is found decreased, whereas the horizontal wave force on the whole foundation and the moment are almost unaffected. This new finding may serve as a good reference to improve the high-rise pile cap structure for future wind farm constructions.

CRediT authorship contribution statement

Ling Chen: Data curation, Writing – original draft, Software, Validation, Visualization. **Jifu Zhou:** Conceptualization, Methodology, Funding acquisition, Project administration, Supervision, Writing – review & editing. **Jinlong Duan:** Writing – review & editing. **Xu Wang:** Methodology, Investigation, Formal analysis.

Declaration of competing interest

The authors declare that they have no known competing financial interests or personal relationships that could have appeared to influence the work reported in this paper.

Acknowledgement

This work was supported by the National Natural Science Foundation of China (Grants 12132018, 11972352), and the Strategic Priority Research Program of the Chinese Academy of Sciences (Grant XDA22040304).

References

Altomare, C., Domínguez, J.M., Crespo, A.J.C., González-Cao, J., Suzuki, T., Gómez-Gesteira, M., Troch, P., 2017. Long-crested wave generation and absorption for SPH-based DualSPHysics model. Coast. Eng. 127, 37–54.
Azadbakht, M., Yim, S.C., 2016. Effect of trapped air on wave forces on coastal bridge superstructures. J. Ocean Eng. Mar. Energy 2 (2), 139–158.
Berberović, E., van Hinsberg, N.P., Jakirlić, S., et al., 2009. Drop impact onto a liquid layer of finite thickness: dynamics of the cavity evolution[J]. Phys. Rev. 79 (3), 036306.
Bredmose, H., Jacobsen, N.G., 2011. Vertical wave impacts on offshore wind turbine inspection platforms. In: ASME 2011 30th Int conf on ocean, offshore and Arctic, pp. 645–654.
Cannata, G., et al., 2019. Numerical investigation of the three-dimensional velocity fields induced by wave-structure interaction. In: ITM Web of Conferences. EDP Sciences, 02011.
Chen, L., Zhou, J.F., Li, J., Lin, Y.F., Li, J.Y., 2016. Monitoring the new fixed offshore wind turbine foundation in the East China Sea. J. Ocean and Wind Energy 3 (1), 10–15.
Chen, L.F., Zang, J., Hillis, A.J., Morgan, G.C.J., Plummer, A.R., 2014. Numerical investigation of wave–structure interaction using OpenFOAM. Coast. Eng. 88, 91–109.
Chen, L., Zhou, J.F., Wang, X., Wang, Z., 2018. Nonlinear wave loads on high-rise pile cap structures in the Donghai bridge wind farm. Int. J. Offshore Polar Eng. 28 (3), 263–271.
Cuomo, G., Shimosako, K.I., Takahashi, S., 2009. Wave-in-deck loads on coastal bridges and the role of air. Coast Eng. 56 (8), 793–809.
Deng, L., Yang, W., Li, Q., Li, A., 2019. CFD investigation of the cap effects on wave loads on piles for the pile-cap foundation[J]. Ocean Eng. 183 (JUL.1), 249–261.
Engsig-Karup, A.P., Bingham, H.B., Lindberg, O., 2009. An efficient flexible-order model for 3D nonlinear water waves. J. Comput. Phys. 228, 2100–2118.
Fenton, J.D., 1988. The numerical solution of steady water wave problems. Comput. Geosci. 14 (3), 357–368.
Hayatdavoodi, M., Seiffert, B., Ertekin, R.C., 2014. Experiments and computations of solitary-wave forces on a coastal-bridge deck. Part II: deck with girders. Coast Eng. 88, 210–228.
Higuera, P., Lara, J.L., Losada, I.J., 2013. Realistic wave generation and active wave absorption for Navier–Stokes models: application to. OpenFOAM. Coast. Eng. 71, 102–118.
Higuera, P., Lara, J.L., Losada, I.J., 2014. Three-dimensional interaction of waves and porous coastal structures using OpenFOAM®. Part I: formulation and validation. Coast Eng. 83, 243–258.
Hirt, C.W., Nichols, B.D., 1981. Volume of fluid (VOF) method for the dynamics of free boundaries. J. Comput. Phys. 39, 201–225.
Hu, Z.Z., Greaves, D., Raby, A., 2016. Numerical wave tank study of extreme waves and wave-structure interaction using OpenFoam. Ocean Eng. 126, 329–342.
Iwanowski, B., Gladsø, R., Lefranc, M., 2009. Wave-in-deck load on a jacket platform, CFD-derived pressures and non-linear structural response. In: ASME 2009 28th International Conference on Ocean. Offshore and Arctic Engineering, pp. 31–40.
Jasak, H., 1996. Error Analysis and Estimation for the Finite Volume Method with Applications to Fluid Flows. University of London. Ph.D. thesis.
Jacobsen, N.G., Fuhrman, D.R., FredsØ, J., 2012. A wave generation toolbox for the open-source CFD library: openfoam. Int. J. Numer. Methods Fluid. 70 (9), 1073–1088.
Kleefsman, K.M.T., Fekken, G., Veldman, A.E.P., Iwanowski, B., Buchner, B., 2005. A volume-of-fluid based simulation method for wave impact problems. J. Comput. Phys. 206 (1), 363–393.
Li, Y., Lin, M., 2012. Regular and irregular wave impacts on floating body. Ocean Eng. 42, 93–101.
Lin, Y.F., 2007. Structure characteristics and design technique keys of turbine foundation in Shanghai Donghai-bridge offshore wind farm. Shanghai Electric Power 2, 153–157 (In Chinese).
Lin, Z., Pokrajac, D., Guo, Y., Jeng, D.S., Tang, T., Rey, N., Zheng, J., Zhang, J., 2017. Investigation of nonlinear wave-induced seabed response around mono-pile foundation. Coast. Eng. 121, 197–211.

Menter, F.R., 1994. Two-equation eddy-viscosity turbulence models for engineering applications. AIAA J. 32, 1598–1605.
Morgan, G.C.J., Zang, J., Greaves, D., Heath, A., Whitlow, C.D., Young, J.R., 2010. Using the RasInterFoam CFD model for wave transformation and coastal modeling. Proc. Coast. Eng. Conf. 9.
Paulsen, B.T., Bredmose, H., Bingham, H.B., 2014a. An efficient domain decomposition strategy for wave loads on surface piercing circular cylinders. Coast. Eng. 86, 57–76.
Paulsen, B.T., Bredmose, H., Bingham, H.B., Jacobsen, N.G., 2014b. Forcing of a bottom-mounted circular cylinder by steep regular water waves at finite depth. J. Fluid Mech. 755, 1–34.
Rusche, H., 2002. Computational Fluid Dynamics of Dispersed Two-phase Flows at High Phase Fractions. PhD Thesis. University of London.
Schellin, T.E., Perić, M., el Moctar, O., 2011. Wave-in-deck load analysis for a jack-up platform. J. Offshore Mech. Arctic Eng. 133 (2), 021303.
Seiffert, B., Hayatdavoodi, M., Ertekin, R.C., 2014. Experiments and computations of solitary-wave forces on a coastal-bridge deck. Part I: flat plate. Coast. Eng. 88, 194–209.
Seiffert, B.R., Ertekin, R.C., Robertson, I.N., 2015. Wave loads on a coastal bridge deck and the role of entrapped air. Appl. Ocean Res. 53, 91–106.
Stansberg, C.T., Baarholm, R., Kristiansen, T., Hansen, E.W.M., Rortveit, G., 2005. Extreme wave amplification and impact loads on offshore structures. In: Offshore Technology Conference. Offshore Technology Conference.
Weller, H.G., Tabor, G., Jasak, H., Fureby, C., 1998. A tensorial approach to computational continuum mechanics using object-oriented techniques. Comput. Phys. 12 (6), 620–631.
Zheng, S.M., Zhang, Y.L., Iglesias, G., 2018. Wave–structure interaction in hybrid wave farms. J. Fluid Struct. 83, 386–412.